

# 3DHumanGAN: Towards Photo-Realistic 3D-Aware Human Image Generation

Zhuoqian Yang<sup>1</sup><sup>1</sup> Shanghai AI Labyangzhuoqian@pjlab.org.cn  
wuwenny0503@gmail.comShikai Li<sup>2</sup><sup>2</sup> SenseTime ResearchWayne Wu<sup>1,2</sup>✉Bo Dai<sup>1</sup>lishikai@sensetime.com  
daibo@pjlab.org.cn

Figure 1. **3DHumanGAN**. View-consistent full-body human images generated by our 3D-aware generative adversarial network (GAN). We show random sampled eight humans, each of them is in three view-angles.

## Abstract

We present **3DHumanGAN**, a 3D-aware generative adversarial network (GAN) that synthesizes images of full-body humans with consistent appearances under different view-angles and body-poses. To tackle the representational and computational challenges in synthesizing the articulated structure of human bodies, we propose a novel generator architecture in which a 2D convolutional backbone is modulated by a 3D pose mapping network. The 3D pose mapping network is formulated as a renderable implicit function conditioned on a posed 3D human mesh. This design has several merits: *i*) it allows us to harness the power of 2D GANs to generate photo-realistic images; *ii*) it generates consistent images under varying view-angles and specifiable poses; *iii*) the model can benefit from the 3D human prior. Our model is adversarially learned from a collection of web images needless of manual annotation. Code and models will be publicly available <sup>12</sup>.

## 1. Introduction

Human image generation is a long-standing topic in computer vision and graphics with countless applications across multiple areas of interest including movie production, social networking and e-commerce. Compared to physically-based methods, data-driven approaches are preferred due to the photo-realism of their results, versatility and ease of use [59]. In this work, we are interested in synthesizing full-body human images with a 3D-aware generative adversarial network (GAN) that produces appearance-consistent images under different view-angles and body-poses.

Rapid developments have been seen in using 3D-aware GANs to generate view-consistent images of human faces [4, 5, 13, 21, 44, 54, 66]. However, these methods have limited capacity when dealt with complex and articulated objects such as human bodies. To begin with, methods based solely on neural volume rendering [5, 44, 54] are too memory inefficient. Rendering human bodies requires a volumetric representation that is much more dense than that of faces, which makes it computationally infeasible. A line of work improves the computational efficiency and rendering quality of 3D-aware GANs by upsampling the rendered result with

<sup>1</sup>Project page: <https://3dhumangan.github.io/>

<sup>2</sup>Code: <https://github.com/3dhumangan/3DHumanGAN>

a convolutional neural network [4, 13, 21, 66]. We argue that this feed-forward approach is not well-suited for generating full-body human images, since the 3D representation is tasked with simultaneously modeling the articulated geometry and the appearance of human bodies, which poses great challenges on representational capacity, while the capacity of the 2D-network is not fully utilized.

As depicted in Figure 2a, our work seeks to solve these problems by introducing a novel generator architecture in which a 2D convolutional backbone is modulated by a 3D pose mapping network. This design is motivated by the observation that in a StyleGAN2 [27] model trained on human images certain layers of styles correlate strongly with the pose of the generated human [10] while others correlate more apparently with the appearance. The 3D Pose Mapping Network is formulated as a renderable implicit function conditioned on a posed 3D human mesh derived with a parametric model [37]. In this way, the 3D representation handles the simplified task of parsing a geometric prior while the network no longer has to learn the articulated body geometry by itself. As an additional benefit of explicitly conditioning on posed human mesh, the pose of the generated human can be specified. The output of the 3D pose mapping network is used to render a 2D low-resolution style map through ray integration [42]. The style map is passed into the first few layers of our backbone network.

Then, we introduce the Appearance Mapping Network to control the appearance of the generated human. The appearance mapping network is formulated as an MLP, following a common practice of style-based generators [26, 27]. For the network to learn to parse the 3D geometric prior, we use a segmentation-based GAN loss [57] calculated using a U-Net [50] discriminator. This design enables the network to establish one-to-many mapping from 3D geometry to synthesized 2D textures using only collections of single-view 2D photographs without manual annotations.

Although capable of producing photo-realistic results, CNN-based generator networks often sacrifice consistency under geometric transformations [4], *i.e.* the appearance of the generated human may change with varying pose and view-angle. To preserve consistency, we propose a network design with two key aspects: 1) Our backbone network is built entirely with  $1 \times 1$  convolutions. This helps eliminate positional reference and promotes equalvariance [25]. 2) Modulation from the pose mapping network is passed into the backbone by means of spatial adaptive batch normalization instead of the commonly used instance normalization [27, 45], so that underlying structure from the geometric information parsed by our pose mapping network is not impaired.

Our contributions can be summarized as follows: 1) Our work is one of the first to achieve 3D-aware generation of photo-realistic full-body human images. 2) We propose a 2D-

3D hybrid generator which is both efficient and expressive. The model is supervised with segmentation-based GAN loss which helps establish a mapping between 3D coordinates and 2D human body semantics. 3) Our generator is carefully designed to preserve the consistency of appearance when pose and view-angle vary.

## 2. Related Works

**3D-Aware Image Generation.** Generative Adversarial Networks [12] are able to generate images of human/animal faces, cars, indoor and natural scenes in eye-fooling photo-realisticness [25–27]. This motivates researchers to explore adversarial learning’s potential in achieving 3D-aware image synthesis. Earlier efforts devised different network structures to process meshes [33, 58], voxels [11, 18, 67] and block-based representations [16, 34]. These methods suffer from the common problem of insufficient 3D inductive bias [4]. Neural implicit representations rendered via ray integration have been found to be an effective representation for data-driven 3D synthesis [36]. Progress was gained in generating objects with simple structure such as human faces [5, 44, 54]. These approaches are burdened by heavy computational cost and limited to generating low-resolution images. Several works propose to remedy this by upsampling the rendered results with a 2D convolutional network and achieved impressive quality [4, 13, 21, 66], yet still not ready for the challenging 3d-aware human image generation. This is because the complexity of the articulated structure of human bodies challenges the 3D representations used by these works.

**Human Image Generation.** Previous works on person image generation focus on re-synthesizing the reference image, such as rendering humans in a novel pose [1, 6, 38, 68], with different garments [15, 31] or with text [23]. Earlier methods condition sparse key-points [38, 39, 48, 51, 68] or semantic maps [7, 14, 62] to manipulate the 2D images. To better preserve the appearance consistency of the source, surface-based methods [1, 32, 35] are introduced to establish the dense correspondences between pixel and human prior surface, *i.e.*, DensePose [49] and SMPL [37]. A limited amount of work focuses on human synthesis without a reference image, where [8] and [52] map the appearance into the Gaussian variables, enabling the synthesis of novel persons. Inspired by the success of StyleGAN [25–27] on unconditional generation, several works [9, 10] explore the capacity of the model for full-body synthesis from different aspects. Specifically, StyleGAN-Human [10] takes a data-centric perspective toward human generation and discusses the effect of manipulated style embedding on human images. Inset-GAN [9] proposes a multi-GAN optimization framework to synthesize more plausible-looking humans. All methods mentioned above are 2D methods.

Three concurrent works [2, 20, 63] tackle 3D-aware human

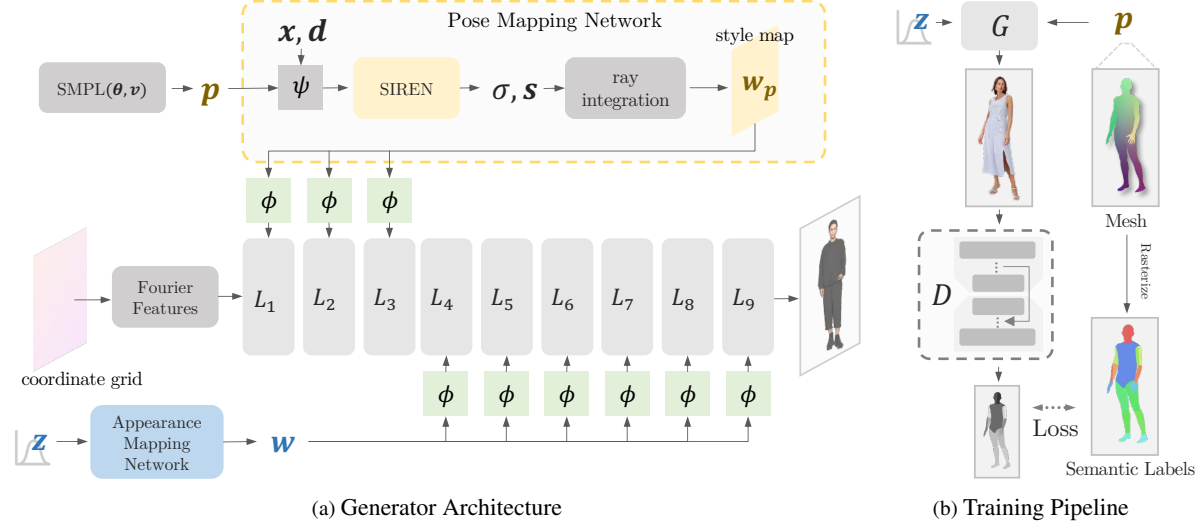


Figure 2. **Architecture.** (a) Our generator uses a pixel-wise independent convolutional backbone modulated by a 3D pose mapping network and an appearance mapping network. (b) Our model is supervised with a segmentation-based GAN loss where the semantic labels are rasterized from the conditioning mesh.

image generation based on different 3D representations. [2] and [63] render a low-resolution image with a 3D triplane representation [4] and uses a 2D convolutional network to enlarge the image in a feed-forward manner. [20] render images directly with an efficient compositional 3D neural field. Our work is different from these works in the following aspects: 1) We use a 2D generator modulated by 3D human body prior instead of directly rendering the image from a 3D representation. 2) We use segmentation-based adversarial supervision which encourages not only fidelity but also semantic correspondence.

### 3. Generator Architecture

We build a generative adversarial network that synthesizes 3D-aware full-body human images with specified pose  $\mathbf{p}$  and view-angle  $\mathbf{v}$ . Pose is specified as a set of coordinates of the vertices in a posed body mesh  $\mathbf{p} = \{\mathbf{v}_i \in \mathbb{R}^3\}_{i=1..6890}$  derived using a parametric human body model SMPL [37]  $\mathbf{p} = \text{SMPL}(\theta, \mathbf{v})$ .  $\theta \in \mathbb{R}^{K \times 4}$  denotes the rotation at each body joint in the quaternion format. The appearance of the generated human is randomly sampled, represented as a vector  $\mathbf{z} \in \mathbb{R}^{N_z}$ , but required to stay consistent when pose and view-angle vary. To this end, we design a 2D-3D-hybrid generator architecture and a training strategy to achieve partially conditioning on pose.

**Architecture.** An overview of our generator is presented in Figure 2a. We use a style-based generator but with a major difference from prior works: different layers of the convolutional backbone are separately modulated by two mapping networks, *i.e.*, a pose mapping network that handles 3D human-body geometry and an appearance mapping network which resembles that of other style-based gener-

ators. This design is motivated by the observation that in a StyleGAN2 [27] model trained on human images. The low-level styles correlate strongly with the pose and orientation of the generated human [10] while others correlate more apparently with the appearance, as shown in Figure 3. This inspires us to inject the human geometric prior by calculating the low-level styles from the conditioning posed mesh.

**3D Pose Mapping Network.** To parse the 3D geometric information, the pose mapping network is formulated as a renderable 3D implicit function  $f_p(\psi(\mathbf{x}|\mathbf{p}, \theta), \mathbf{d}) = (\sigma, \mathbf{s}_x)$  where  $\mathbf{x} \in \mathbb{R}^3$  is a coordinate in the 3D camera space;  $\mathbf{d} \in \mathbb{R}^3$  denotes the orientation of the camera ray;  $\mathbf{p} \in \mathbb{R}^{6890 \times 3}$  denotes the coordinates of the body vertices in camera space;  $\psi(\mathbf{x}|\mathbf{p}, \theta)$  transforms the coordinate  $\mathbf{x}$  from the camera space to a canonical space, added to facilitate learning. Following literature in 3D human body reconstruction [41, 47, 65],  $\psi$  is defined as the inverse process of linear blend skinning,

$$\psi(\mathbf{x}|\mathbf{p}, \theta) = \left( \sum_{k=1}^K \omega_k(\mathbf{x}, \mathbf{p}) \mathbf{G}_k(\theta) \right)^{-1} \mathbf{x}$$

$\omega_k(\mathbf{x}, \mathbf{p})$  returns the blend weights corresponding to the vertex nearest to the querying point  $\mathbf{x}$ ;  $\mathbf{G}_k(\theta) \in \text{SE}(3)$  denotes the cumulative linear transformation at the  $k^{\text{th}}$  skeleton joint. The outputs of the implicit function are the opacity  $\sigma \in \mathbb{R}$  and a style vector  $\mathbf{s} \in \mathbb{R}^{N_s}$ , which are used to render a 2D low-resolution pose style map  $\mathbf{w}_s \in \mathbb{R}^{H_s \times W_s \times N_s}$  via ray integration [42]. The implicit function is parameterized as an MLP with periodic activation [56] to handle low-dimensional coordinate input.



Figure 3. **Style mixing with StyleGAN2.** The source and reference images are randomly generated using StyleGAN2. Style mixing is to replace to part of the style vectors from the source image with their counterparts from the reference images. *Low*-level styles modulate the first few layers of the StyleGAN2 generator while *high*-level styles modulate the last few layers.

**Neural Rendering.** We use classic volume rendering technique to aggregate predicted style vectors across space. We start by evenly sampling  $N$  points  $\{\mathbf{x}_i = \mathbf{o} + t_i \mathbf{d}\}$  within near and far bounds  $[t_n, t_f]$  along each camera ray  $\mathbf{r}(t) = \mathbf{o} + t \mathbf{d}$ .  $\mathbf{o}$  denotes the camera center. The style vector on each 2D spatial location is then estimated via

$$\mathbf{S}(\mathbf{r}) = \sum_{i=1}^N T_i (1 - \exp(-\sigma(\mathbf{x}_i) \delta_i)) \mathbf{s}(\mathbf{x}_i, \mathbf{d}),$$

$$T_i = \exp \left( - \sum_{j=1}^{i-1} \sigma(\mathbf{x}_j) \delta_j \right),$$

where  $\delta_i = |\mathbf{x}_{i+1} - \mathbf{x}_i|$  denotes the distance between adjacent samples.

**Appearance Mapping Network.** The appearance mapping network is an MLP  $f_a(\mathbf{z}) = \mathbf{w} \in \mathbb{R}^{N_w}$ , following common practice of style-based generators [25–27]. The output style vectors  $\mathbf{w}$  do not have spatial dimensions. The final output image is synthesized by the convolutional backbone under modulation from both mapping networks.

## 4. Training

Our training pipeline is illustrated in Figure 2b. For the network to learn to parse the 3D geometric prior and synthesize images with specified pose, a mapping from 3D geometric information to 2D textures needs to be established.

Inspired by [53], we use a U-Net [50] discriminator architecture together with a segmentation-based GAN loss to establish a one-to-many mapping between geometry and textures. Specifically, the U-Net discriminator classifies each pixel as *fake*, *background* or one of 25 semantic classes (e.g. *head*, *torso* ...), unlike the binary classification on entire images used in traditional GAN training. This approach simultaneously enables free appearance sampling and pose conditioning. A popular practices in pose-conditioned human image generation it to use VAE-style supervision, but the quality of generated image is often outperformed by that of GAN-style training [9]. When updating the discriminator, triplets of real images, corresponding SMPL meshes and semantic label maps ( $\mathbf{I}$ ,  $\mathbf{p}_\mathbf{I}$ ,  $\mathbf{m}_\mathbf{I}$ ) are needed to calculate the loss.

$$\mathcal{L}_{\text{adv}}^D = -\mathbb{E}_{\mathbf{I}} \left[ \sum_c^{N_c} \alpha_c \sum_{x,y}^{H \times W} \mathbf{m}_{\mathbf{I},x,y,c} \log D(\mathbf{I})_{x,y,c} \right]$$

$$- \mathbb{E}_{\mathbf{p},\mathbf{z}} \left[ \sum_c^{N_c} \alpha_c \sum_{x,y}^{H \times W} \mathbf{m}_{\mathbf{0},x,y,c} \log D(G(\mathbf{p}, \mathbf{z}))_{x,y,c} \right]$$

where  $x$ ,  $y$  and  $c$  are subscripts of the height, width and class dimension.  $\alpha_c$  denotes class weights, calculated as the inverse of the per-pixel class frequency.  $\mathbf{m}_0$  denotes a semantic label map in which everywhere is 0, corresponding to the *fake* class. When updating the generator, pairs of SMPL meshes and semantic label maps ( $\mathbf{p}$ ,  $\mathbf{m}_\mathbf{p}$ ) are required.

$$\mathcal{L}_{\text{adv}}^G = -\mathbb{E}_{\mathbf{p},\mathbf{z}} \left[ \sum_c^{N_c} \alpha_c \sum_{x,y}^{H \times W} \mathbf{m}_{\mathbf{p},x,y,c} \log D(G(\mathbf{p}, \mathbf{z}))_{x,y,c} \right]$$

The segmentation-based GAN loss is sufficient for training the model to generate consistent images with desired pose and view-angle. In practice, we find adding two additional loss terms improves image quality. The first is a perceptual loss [24] which minimizes the difference between feature activations extracted from real and generated images using a pretrained VGG [55] network.

$$\mathcal{L}_{\text{perceptual}}^G = |\text{VGG}(G(\mathbf{p}_\mathbf{I}, \hat{\mathbf{z}}_\mathbf{I})) - \text{VGG}(\mathbf{I})|$$

where  $\hat{\mathbf{z}}_\mathbf{I}$  is an appearance latent code corresponding with the groundtruth image  $\mathbf{I}$ . These appearance codes are learnable parameters in the model, initialized by inverting a pretrained StyleGAN2 model [10] with e4e [60]. During training, the collection of appearance latent codes are optimized but anchored by a latent loss.

$$\mathcal{L}_{\text{latent}}^G = |\hat{\mathbf{z}}_\mathbf{I} - \text{e4e}(\mathbf{I})|$$

It is reported that gradient penalty on the discriminator facilitates stable training and convergence [27, 40]. We implement an R1 regularization for our segmentation-based GAN loss:

$$\mathcal{L}_{R1}^D = \frac{\gamma}{2} \mathbb{E}_{\mathbf{I}} \|\nabla_{\mathbf{I}} D(\mathbf{I})\|^2$$

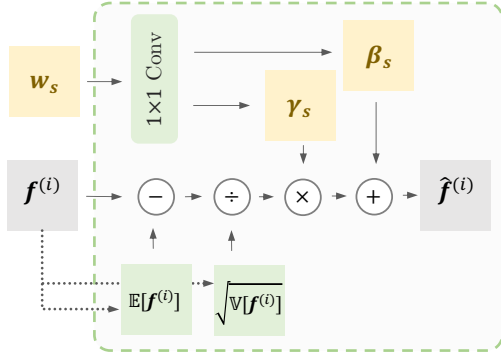


Figure 4. **Spatial adaptive batch normalization** first performs a statistics-based per-channel normalization on the feature maps and then a re-normalization with mean and variance values calculated from the style maps.

The total loss for training the generator is the sum of the above terms.

$$\mathcal{L}^G = \lambda_{\text{adv}} \mathcal{L}_{\text{adv}}^G + \lambda_{\text{perceptual}} \mathcal{L}_{\text{perceptual}}^G + \lambda_{\text{latent}} \mathcal{L}_{\text{latent}}^G + \gamma \mathcal{L}_{R1}^D$$

## 5. Preserving Consistency

Although capable of producing high-quality results, CNN-based generator networks often sacrifice consistency under geometric transformations [4]. This is a crucial challenge in our approach. Our network is carefully designed to preserve the consistency of appearance against varying pose and view-angle.

**Pixel-wise independent convolutional backbone.** Our backbone network is based entirely on  $1 \times 1$  convolutions and no upsampling is used. The input to the backbone network is a constant coordinate grid  $\mathbf{g} \in \mathbb{R}^{H \times W \times 2}$  containing normalized screen coordinates ranged  $[-1, 1]$ . Thereby, each pixel is synthesized independent of others. The purpose of this is to eliminate unwanted positional references so that the network is equal-variant to geometric transformations [25].

**Spatial-adaptive batch normalization.** The spatial adaptive batch normalization which is used to pass the style maps into the backbone in a way that does not impair underlying structure. Let us denote by  $\mathbf{f}^{(i)}$  the output feature map of the  $i^{th}$  layer of the backbone. A spatial adaptive normalization [45] function  $\phi(\mathbf{f}^{(i)}, \mathbf{w}_s) = \hat{\mathbf{f}}^{(i)}$  is needed to inject the style maps rendered by our pose mapping network into the feature maps. As shown in Figure 4, spatial adaptive normalization first performs a statistics-based per-channel normalization on the feature maps and then a re-normalization with mean and variance values calculated from the style maps. In the first normalization step, how the statistics are calculated makes a crucial difference. When the statistics are calculated on individual feature maps in a mini-batch, *i.e.* instance normalization [61], which is used by [26, 45], consistency is impaired. We hypothesize that this is because instance normalization removes global affine transformation

applied by the previous spatial normalization and forces the normalized layer to resort to controlling only the presence of finer features rather than their precise positions, as similarly observed in [25]. We propose to use *spatial adaptive batch normalization*:

$$\phi(\mathbf{f}_{x,y,c}^{(i)}, \mathbf{s}) = \gamma^{(i)}(\mathbf{s})_{x,y,c} \cdot \frac{\mathbf{f}_{x,y,c}^{(i)} - \mathbb{E}_{\mathbf{p}, \mathbf{z}}[\mathbf{f}_{x,y,c}^{(i)}]}{\sqrt{\mathbb{V}_{\mathbf{p}, \mathbf{z}}[\mathbf{f}_{x,y,c}^{(i)}]}} + \beta^{(i)}(\mathbf{s})_{x,y,c}$$

where  $x, y$  and  $c$  are the subscripts for the width, height and channel dimension.  $\gamma^{(i)}$  and  $\beta^{(i)}$  are learned affine transformations.  $\mathbb{E}$  and  $\mathbb{V}$  estimates the means and variances of the activations of a feature channel across all pixels and all combinations of poses, views and appearances. In practice, this is done by keeping track of the mini-batch statistics of the per-channel activations through exponential moving average. Spatial adaptive batch normalization is used throughout the generation pipeline. For the style vectors  $\mathbf{w}$  calculated with the appearance network, the same re-normalization is broadcasted to all spatial locations.

## 6. Experiments

**Dataset.** We compare 3D-aware human image generation performance on SHHQ [10], a collection of  $\sim 220k$  real-world full-body human images. All compared models are trained on this dataset. We use an off-the-shelf model PARE [29] to register a SMPL mesh for each of the training images. The semantic label maps are then obtained by rasterizing the conditioning posed mesh (mapping between mesh vertices and semantic labels is known). We augment the semantic label maps with estimations from a 2D semantic segmentation method DensePose [49]. The latter's results are better aligned with the images compared to the estimations from PARE. During training, pose, view and appearance are independently sampled. Poses are directly sampled from data. The view angle is sampled from a normal distribution set according to dataset statistics *i.e.* yaw  $\sim \mathcal{N}(0, 0.4)$  and pitch  $\sim \mathcal{N}(0, 0.06)$ .

**Baselines.** We compare with a 2D unconditional method StyleGAN2 [27], a 2D conditional method OASIS [53] and 3D-aware unconditional methods StyleNeRF [13] and EG3D [4]. Note that we do not compare with purely-3D methods such as [5, 44, 54] because these methods do not support training at a reasonable resolution. To evaluate and compare the pose-conditioning capability, we implement pose conditioning for the unconditional methods by first inverting a human image with desired pose to the style-space and then mixing these style vectors with the ones calculated from the randomly sampled  $\mathbf{z}$ . For StyleGAN2, the inversion method used is e4e [60]. For StyleNeRF and EG3D, we train a ResNet [17] encoder to infer the latent code given camera parameters.



Figure 5. **Qualitative Results.** In (a), each row shows two cases separated by the dotted line. For each case we show one identity in two poses and three view-angles. The conditioning mesh is shown on the left of each case. (b) shows two cases of appearance interpolation. (c) shows two cases of pose interpolation.

**Evaluation Metrics.** We evaluate three main criteria of the generated results, i.e. fidelity, accuracy of pose conditioning and consistency. We measure fidelity with Fréchet inception distance [19] and kernel inception distance [3]. Two sets of fidelity metrics are calculated for unconditional generation and pose-conditional generation, denoted as (*FID-u*, *KID-u*) and (*FID-p*, *KID-p*), respectively. These values are calculated between 50,000 real and generated images using an alias-free implementation [46]. To evaluate the accuracy of generated pose under conditioning, we use PARE [30] to re-estimate pose from generated images and calculate the 2D mean per-joint position error [22] in normalized screen space ranged  $[-1, 1]$ . We measure the consistency of appearance under varying pose and view-angle using the signal restoration metric peak signal-to-noise ratio (PSNR) in decibels (dB), following [25, 64]. Specifically, we use the conditioning 3D SMPL mesh to perform a reverse mapping from pixels to mesh vertices. The PSNR is then calculated between corresponding vertices on these colored meshes. The *Con-v* and *Con-p* respectively denote PSNR calculated under view change and pose change.

Table 1. **Quantitative Comparisons** on human images generated by 2D and 3D methods. *KID* values are reported in  $10^{-3}$  units; *Pose* values are reported in  $10^{-2}$  units. Our method achieves the lowest fidelity scores and the highest score of appearance consistency under different body-poses.

| Metrics | StyleGAN-Human, 512 | OASIS, 256  | StyleNeRF, 512 | EG3D, 512 | Ours, 256   | Ours, 512    |
|---------|---------------------|-------------|----------------|-----------|-------------|--------------|
| FID-p   | 6.68                | 10.74       | 13.13          | 26.75     | <b>6.61</b> | 9.31         |
| KID-p   | 3.60                | 8.82        | 7.01           | 19.70     | <b>3.01</b> | 5.16         |
| FID-u   | <b>2.83</b>         | -           | 7.6            | 17.83     | -           | -            |
| KID-u   | <b>1.50</b>         | -           | 3.96           | 11.74     | -           | -            |
| Pose    | 4.48                | <b>1.82</b> | 6.64           | 8.22      | 2.21        | 2.08         |
| Con-v   | -                   | -           | 18.29          | 19.93     | 21.83       | <b>22.66</b> |
| Con-p   | 12.77               | 13.19       | 13.74          | 10.66     | 17.72       | <b>18.58</b> |

## 6.1. Qualitative Results

Figure 5a shows 3D-aware human image generation results in multiple poses and view-angles. The appearances of the humans generated with our method is consistent under view and pose changes. Figure 5b and 5c show the interpolation results. Our model is able to generate smooth interpolation of appearance and pose.



Figure 6. **Qualitative Comparison.** We show two cases separated by the dotted line. For each case, the first row shows unconditional generation results, the second row shows pose-conditional generation results. We show three view angles, from  $-30^\circ$  to  $30^\circ$ .

Table 2. **Ablation study** quantitative results. *KID* values are reported in  $10^{-3}$  units; *Pose* values are reported in  $10^{-2}$  units.

| Metrics | VAE   | Feed Forward | Upsampling  | Instance Norm | Full         |
|---------|-------|--------------|-------------|---------------|--------------|
| FID-p   | 8.00  | 9.42         | 8.28        | 8.90          | <b>6.61</b>  |
| KID-p   | 4.02  | 4.57         | 5.42        | 4.04          | <b>3.01</b>  |
| Pose    | 9.54  | 2.60         | <b>1.89</b> | 1.93          | 2.21         |
| Con-v   | 19.22 | 21.63        | 16.03       | 17.73         | <b>21.83</b> |
| Con-p   | 15.18 | <b>17.89</b> | 13.16       | 13.36         | 17.72        |

## 6.2. Comparisons

Quantitative results are presented in Table 1. Qualitative results are shown in Figure 6. Our method demonstrates the best overall performance, with an FID comparable to the 2D state-of-the-art method StyleGAN-Human and the best consistency. With GAN inversion techniques applied, the unconditional StyleGAN2, StyleNeRF and EG3D are able to generate images where the target pose is close to the condition but with some gaps. This suggests that the

representations learned by these methods are entangled in appearance and pose. Style mixing is not enough to achieve clean separation in the two domains. Our method is able to generate images that accurately matches the conditioning pose. Besides, all of the compared baselines show different extents of inconsistencies under view and pose variation. This is an indicator of entanglement of appearance and pose in the learned latent spaces of the baselines. In contrast, the appearance of the humans generated by our method remains consistent under pose and view variation.

## 6.3. Ablation Study

To assess the effectiveness of each designed module in our 3d-aware generator, we evaluate a set of ablated models where the modules to be evaluated are replaced with approaches used by previous works. Specifically, to examine the effects of passing the 3D geometric prior into the 2D backbone as styles, i.e. the 2D-3D hybrid generator, we compare with the feed-forward approach used by [4, 13, 66], denoted as (*Feed Forward*). To evaluate the contribution

of the segmentation-based GAN loss, we train a model in which this loss is replaced with the traditional GAN loss with binary discrimination. This results in a model trained under VAE-style supervision as in [21], denoted as *VAE*. To examine the effectiveness of the pixel-independent backbone design, we compare with a variant that uses traditional upsampling convolution network like in [27, 53], which is denoted as *Upsampling*. To examine the effectiveness of spatial adaptive batch normalization, we compare with a variant that uses spatial adaptive instance normalization instead, denoted as *Instance Norm*. All ablation models are trained and evaluate in the resolution of  $256 \times 128$ . Quantitative results are presented in Table 2 and qualitative results are presented in the appendix. Our full model performs best in fidelity and view-consistency. The *Feed-Forward* approach slightly outperforms the full model in consistency, but with no small sacrifice in image quality. In other terms, passing the geometric prior in the form of low-level styles has a small toll on pose-accuracy and consistency, but completely within the acceptable range. Meanwhile, the image quality is greatly improved. By examining the results of the *VAE* setting, we can see that segmentation-based GAN loss is crucial to pose accuracy. It also improves fidelity, possibly because this loss helps the model to make better use of the 3D Human Prior. The *Upsampling* and *Instance Norm* configurations show the best accuracy of generated pose but with impaired image consistency in different extents. These two configurations show that the pixel-wise independent backbone and spatial adaptive batch normalization indeed preserves consistency.

#### 6.4. Internal Representation

Figure 7 visualizes typical internal representations from our networks. One interesting observation is that in the model that uses batch normalization, we are able to find certain feature activations that are consistent across different poses, view-angles and appearances, such as the ones depicted. In contrast, activations of such kind cannot be found in the model that uses instance normalization. One explanation is that the feature activations in the instance normalization model mainly controls the presence of image features rather than the location, which is similarly reported in [25]. We believe an internal coordinate system is preserved when using batch normalization and this helps locate different image textures on the 3D surface, which certainly helps image consistency.

#### 6.5. Limitations and Discussion

Our network still generates some artifacts (see Figure 6) when we rotate by a large angle. Part of the reason is that the dataset features a narrow distribution of view-angles. Another observation is that there are small inconsistencies in the appearance when the view-angle changes. (see Figure 5). Therefore, our method can still be improved in terms of view-consistency.

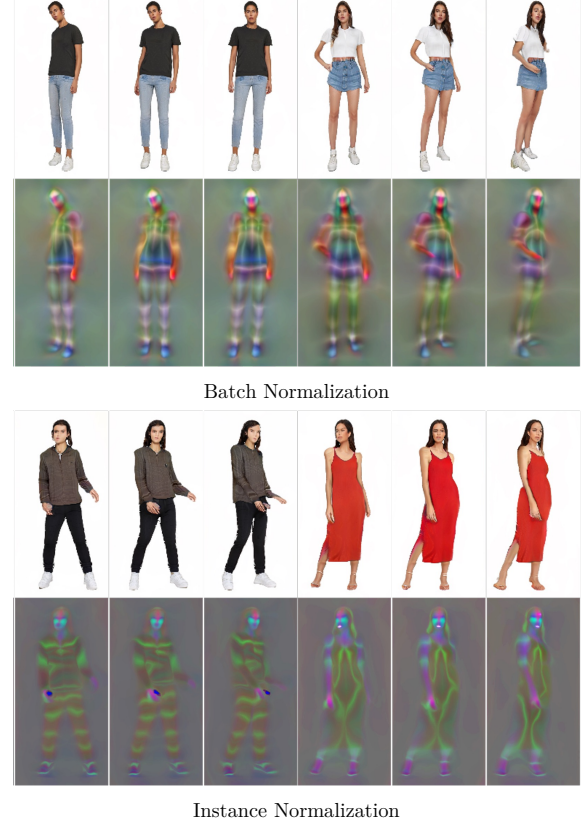


Figure 7. **Internal Representation Visualization.** Two identities in two different poses are visualized for each model. For the same model, the same feature channel are shown for the two identities.

## 7. Conclusion

We build one of the first generative adversarial networks 3DHumanGAN that achieves 3D-aware synthesis of full-body human images. Our 2D-3D hybrid generator effectively and efficiently uses 3D geometric prior of the human body and achieves consistent appearance under varying poses and view-angles with competitive image quality. Our segmentation-based GAN loss plays an irreplaceable role in teaching the generator to parse and condition on the 3D human body prior. By examining ablated models and visualizing internal representation, we find that our pixel-independent backbone together with the spatial adaptive batch normalization technique preserve consistency by keeping the underlying structures inferred from the 3D geometric priors intact.

## References

- [1] Badour Albahar, Jingwan Lu, Jimei Yang, Zhixin Shu, Eli Shechtman, and Jia-Bin Huang. Pose with style: Detail-preserving pose-guided image synthesis with conditional StyleGAN. *ACM TOG*, 2021. 2
- [2] Alexander W Bergman, Petr Kellnhofer, Yifan Wang, Eric R

Chan, David B Lindell, and Gordon Wetzstein. Generative neural articulated radiance fields. *arXiv preprint arXiv:2206.14314*, 2022. 2, 3

[3] Mikołaj Bińkowski, Danica J Sutherland, Michael Arbel, and Arthur Gretton. Demystifying mmd gans. *arXiv preprint arXiv:1801.01401*, 2018. 6

[4] Eric R Chan, Connor Z Lin, Matthew A Chan, Koki Nagano, Boxiao Pan, Shalini De Mello, Orazio Gallo, Leonidas Guibas, Jonathan Tremblay, Sameh Khamis, et al. Efficient geometry-aware 3d generative adversarial networks. *arXiv preprint arXiv:2112.07945*, 2021. 1, 2, 3, 5, 7

[5] Eric R Chan, Marco Monteiro, Petr Kellnhofer, Jiajun Wu, and Gordon Wetzstein. pi-gan: Periodic implicit generative adversarial networks for 3d-aware image synthesis. In *CVPR*, 2021. 1, 2, 5

[6] Wei Cheng, Su Xu, Jingtian Piao, Chen Qian, Wayne Wu, Kwan-Yee Lin, and Hongsheng Li. Generalizable neural performer: Learning robust radiance fields for human novel view synthesis. *arXiv preprint arXiv:2204.11798*, 2022. 2

[7] Haoye Dong, Xiaodan Liang, Ke Gong, Hanjiang Lai, Jia Zhu, and Jian Yin. Soft-gated warping-gan for pose-guided person image synthesis. 2018. 2

[8] Patrick Esser, Ekaterina Sutter, and Björn Ommer. A variational u-net for conditional appearance and shape generation. In *CVPR*, 2018. 2

[9] Anna Frühstück, Krishna Kumar Singh, Eli Shechtman, Niloy J Mitra, Peter Wonka, and Jingwan Lu. Inset-GAN for full-body image generation. *arXiv preprint arXiv:2203.07293*, 2022. 2, 4

[10] Jianglin Fu, Shikai Li, Yuming Jiang, Kwan-Yee Lin, Chen Qian, Chen-Change Loy, Wayne Wu, and Ziwei Liu. Stylegan-human: A data-centric odyssey of human generation. *arXiv preprint arXiv:2204.11823*, 2022. 2, 3, 4, 5

[11] Matheus Gadelha, Subhransu Maji, and Rui Wang. 3d shape induction from 2d views of multiple objects. In *3DV*, 2017. 2

[12] Ian Goodfellow, Jean Pouget-Abadie, Mehdi Mirza, Bing Xu, David Warde-Farley, Sherjil Ozair, Aaron Courville, and Yoshua Bengio. Generative adversarial nets. *NeurIPS*, 2014. 2

[13] Jiatao Gu, Lingjie Liu, Peng Wang, and Christian Theobalt. Stylernerf: A style-based 3d-aware generator for high-resolution image synthesis. In *ICLR*, 2022. 1, 2, 5, 7

[14] Xintong Han, Xiaojun Hu, Weilin Huang, and Matthew R Scott. Clothflow: A flow-based model for clothed person generation. In *ICCV*, 2019. 2

[15] Xintong Han, Zuxuan Wu, Zhe Wu, Ruichi Yu, and Larry S Davis. VITON: An image-based virtual Try-On network. In *CVPR*, 2018. 2

[16] Zekun Hao, Arun Mallya, Serge Belongie, and Ming-Yu Liu. Gancraft: Unsupervised 3d neural rendering of minecraft worlds. In *ICCV*, 2021. 2

[17] Kaiming He, Xiangyu Zhang, Shaoqing Ren, and Jian Sun. Deep residual learning for image recognition. In *CVPR*, 2016. 5

[18] Philipp Henzler, Niloy J Mitra, and Tobias Ritschel. Escaping plato’s cave: 3d shape from adversarial rendering. In *ICCV*, 2019. 2

[19] Martin Heusel, Hubert Ramsauer, Thomas Unterthiner, Bernhard Nessler, and Sepp Hochreiter. Gans trained by a two time-scale update rule converge to a local nash equilibrium. *Advances in neural information processing systems*, 30, 2017. 6

[20] Fangzhou Hong, Zhaoxi Chen, Yushi Lan, Liang Pan, and Ziwei Liu. Eva3d: Compositional 3d human generation from 2d image collections. *arXiv preprint arXiv:2210.04888*, 2022. 2, 3

[21] Yang Hong, Bo Peng, Haiyao Xiao, Ligang Liu, and Juyong Zhang. Headnerf: A real-time nerf-based parametric head model. *arXiv preprint arXiv:2112.05637*, 2021. 1, 2, 8

[22] Catalin Ionescu, Dragos Papava, Vlad Olaru, and Cristian Sminchisescu. Human3. 6m: Large scale datasets and predictive methods for 3d human sensing in natural environments. *TPAMI*, 2013. 6

[23] Yuming Jiang, Shuai Yang, Haonan Qiu, Wayne Wu, Chen Change Loy, and Ziwei Liu. Text2human: Text-driven controllable human image generation. *ACM Transactions on Graphics (TOG)*, 41(4):1–11, 2022. 2

[24] Justin Johnson, Alexandre Alahi, and Li Fei-Fei. Perceptual losses for real-time style transfer and super-resolution. In *ECCV*, 2016. 4

[25] Tero Karras, Miika Aittala, Samuli Laine, Erik Härkönen, Janne Hellsten, Jaakko Lehtinen, and Timo Aila. Alias-free generative adversarial networks. 2021. 2, 4, 5, 6, 8

[26] Tero Karras, Samuli Laine, and Timo Aila. A style-based generator architecture for generative adversarial networks. In *CVPR*, 2019. 2, 4, 5

[27] Tero Karras, Samuli Laine, Miika Aittala, Janne Hellsten, Jaakko Lehtinen, and Timo Aila. Analyzing and improving the image quality of StyleGAN. In *CVPR*, 2020. 2, 3, 4, 5, 8

[28] Diederik P Kingma and Jimmy Ba. Adam: A method for stochastic optimization. *arXiv preprint arXiv:1412.6980*, 2014.

[29] Muhammed Kocabas, Chun-Hao P Huang, Otmar Hilliges, and Michael J Black. Pare: Part attention regressor for 3d human body estimation. In *CVPR*, 2021. 5

[30] Muhammed Kocabas, Chun-Hao P. Huang, Otmar Hilliges, and Michael J. Black. PARE: Part attention regressor for 3D human body estimation. In *ICCV*, 2021. 6

[31] Kathleen M Lewis, Srivatsan Varadharajan, and Ira Kemelmacher-Shlizerman. TryOnGAN: Body-aware Try-On via layered interpolation. *ACM TOG*, 2021. 2

[32] Yining Li, Chen Huang, and Chen Change Loy. Dense intrinsic appearance flow for human pose transfer. In *CVPR*, 2019. 2

[33] Yiyi Liao, Katja Schwarz, Lars Mescheder, and Andreas Geiger. Towards unsupervised learning of generative models for 3d controllable image synthesis. In *CVPR*, 2020. 2

[34] Lingjie Liu, Jiatao Gu, Kyaw Zaw Lin, Tat-Seng Chua, and Christian Theobalt. Neural sparse voxel fields. *NeurIPS*, 2020. 2

[35] Wen Liu, Zhixin Piao, Min Jie, Wenhan Luo, Lin Ma, and Shenghua Gao. Liquid warping gan: A unified framework for human motion imitation, appearance transfer and novel view synthesis. In *ICCV*, 2019. 2

[36] Stephen Lombardi, Tomas Simon, Jason Saragih, Gabriel Schwartz, Andreas Lehrmann, and Yaser Sheikh. Neural volumes: Learning dynamic renderable volumes from images. *arXiv preprint arXiv:1906.07751*, 2019. 2

[37] Matthew Loper, Naureen Mahmood, Javier Romero, Gerard Pons-Moll, and Michael J. Black. SMPL: A skinned multi-person linear model. *ACM TOG*, 2015. 2, 3

[38] Liqian Ma, Xu Jia, Qianru Sun, Bernt Schiele, Tinne Tuytelaars, and Luc Van Gool. Pose guided person image generation. *arXiv preprint*, arXiv:1705.09368, 2017. 2

[39] Liqian Ma, Qianru Sun, Stamatios Georgoulis, Luc Van Gool, Bernt Schiele, and Mario Fritz. Disentangled person image generation. In *CVPR*, 2018. 2

[40] Lars Mescheder, Andreas Geiger, and Sebastian Nowozin. Which training methods for gans do actually converge? In *International conference on machine learning*, pages 3481–3490. PMLR, 2018. 4

[41] Marko Mihajlovic, Yan Zhang, Michael J Black, and Siyu Tang. Leap: Learning articulated occupancy of people. In *CVPR*, 2021. 3

[42] Ben Mildenhall, Pratul P Srinivasan, Matthew Tancik, Jonathan T Barron, Ravi Ramamoorthi, and Ren Ng. Nerf: Representing scenes as neural radiance fields for view synthesis. In *ECCV*, 2020. 2, 3

[43] Takeru Miyato, Toshiki Kataoka, Masanori Koyama, and Yuichi Yoshida. Spectral normalization for generative adversarial networks. *arXiv preprint arXiv:1802.05957*, 2018.

[44] Michael Niemeyer and Andreas Geiger. Giraffe: Representing scenes as compositional generative neural feature fields. In *CVPR*, 2021. 1, 2, 5

[45] Taesung Park, Ming-Yu Liu, Ting-Chun Wang, and Jun-Yan Zhu. Semantic image synthesis with spatially-adaptive normalization. In *CVPR*, 2019. 2, 5

[46] Gaurav Parmar, Richard Zhang, and Jun-Yan Zhu. On aliased resizing and surprising subtleties in gan evaluation. In *Proceedings of the IEEE/CVF Conference on Computer Vision and Pattern Recognition*, pages 11410–11420, 2022. 6

[47] Sida Peng, Junting Dong, Qianqian Wang, Shangzhan Zhang, Qing Shuai, Hujun Bao, and Xiaowei Zhou. Animatable neural radiance fields for human body modeling. In *ICCV*, 2021. 3

[48] Yurui Ren, Xiaoming Yu, Junming Chen, Thomas H Li, and Ge Li. Deep image spatial transformation for person image generation. 2020. 2

[49] Iasonas Kokkinos Riza Alp Güler, Natalia Neverova. Densepose: Dense human pose estimation in the wild. 2018. 2, 5

[50] Olaf Ronneberger, Philipp Fischer, and Thomas Brox. U-net: Convolutional networks for biomedical image segmentation. In *MICCAI*, 2015. 2, 4

[51] Kripasindhu Sarkar, Vladislav Golyanik, Lingjie Liu, and Christian Theobalt. Style and pose control for image synthesis of humans from a single monocular view. *arXiv preprint*, arXiv:2102.11263, 2021. 2

[52] Kripasindhu Sarkar, Lingjie Liu, Vladislav Golyanik, and Christian Theobalt. HumanGAN: A generative model of human images. In *3DV*, 2021. 2

[53] Edgar Schönenfeld, Vadim Sushko, Dan Zhang, Juergen Gall, Bernt Schiele, and Anna Khoreva. You only need adversarial supervision for semantic image synthesis. In *ICLR*, 2021. 4, 5, 8

[54] Katja Schwarz, Yiyi Liao, Michael Niemeyer, and Andreas Geiger. Graf: Generative radiance fields for 3d-aware image synthesis. *NeurIPS*, 2020. 1, 2, 5

[55] Karen Simonyan and Andrew Zisserman. Very deep convolutional networks for large-scale image recognition. *arXiv preprint arXiv:1409.1556*, 2014. 4

[56] Vincent Sitzmann, Julien Martel, Alexander Bergman, David Lindell, and Gordon Wetzstein. Implicit neural representations with periodic activation functions. *NeurIPS*, 2020. 3

[57] Vadim Sushko, Edgar Schönenfeld, Dan Zhang, Juergen Gall, Bernt Schiele, and Anna Khoreva. You only need adversarial supervision for semantic image synthesis. *arXiv preprint arXiv:2012.04781*, 2020. 2

[58] Attila Szabó, Givi Meishvili, and Paolo Favaro. Unsupervised generative 3d shape learning from natural images. *arXiv preprint arXiv:1910.00287*, 2019. 2

[59] Ayush Tewari, Ohad Fried, Justus Thies, Vincent Sitzmann, Stephen Lombardi, Kalyan Sunkavalli, Ricardo Martin-Brualla, Tomas Simon, Jason Saragih, Matthias Nießner, et al. State of the art on neural rendering. In *CGF*, 2020. 1

[60] Omer Tov, Yuval Alaluf, Yotam Nitzan, Or Patashnik, and Daniel Cohen-Or. Designing an encoder for stylegan image manipulation. *ACM TOG*, 2021. 4, 5

[61] Dmitry Ulyanov, Andrea Vedaldi, and Victor Lempitsky. Instance normalization: The missing ingredient for fast stylization. *arXiv preprint arXiv:1607.08022*, 2016. 5

[62] Zhuoqian Yang, Wentao Zhu, Wayne Wu, Chen Qian, Qiang Zhou, Bolei Zhou, and Chen Change Loy. Transmomo: Invariance-driven unsupervised video motion retargeting. In *CVPR*, 2020. 2

[63] Jianfeng Zhang, Zihang Jiang, Dingdong Yang, Hongyi Xu, Yichun Shi, Guoxian Song, Zhongcong Xu, Xinchao Wang, and Jiashi Feng. Avatargen: a 3d generative model for animatable human avatars. *arXiv preprint arXiv:2208.00561*, 2022. 2, 3

[64] Richard Zhang. Making convolutional networks shift-invariant again. In *ICML*, 2019. 6

[65] Fuqiang Zhao, Wei Yang, Jiakai Zhang, Pei Lin, Yingliang Zhang, Jingyi Yu, and Lan Xu. Humannerf: Generalizable neural human radiance field from sparse inputs. *arXiv preprint arXiv:2112.02789*, 2021. 3

[66] Peng Zhou, Lingxi Xie, Bingbing Ni, and Qi Tian. CIPS-3D: A 3d-aware generator of gans based on conditionally-independent pixel synthesis. *arXiv preprint*, arXiv:2110.09788, 2021. 1, 2, 7

[67] Jun-Yan Zhu, Zhoutong Zhang, Chengkai Zhang, Jiajun Wu, Antonio Torralba, Josh Tenenbaum, and Bill Freeman. Visual object networks: Image generation with disentangled 3d representations. *NeurIPS*, 2018. 2

[68] Zhen Zhu, Tengteng Huang, Baoguang Shi, Miao Yu, Bofei Wang, and Xiang Bai. Progressive pose attention transfer for person image generation. In *CVPR*, 2019. 2